A Physiologic Imaging Pilot Study of Breast Cancer Treated with AZD2171

Kathy D. Miller,[1] Michael Miller,[2] Sanjana Mehrotra,[3] Beamon Agarwal,[3] Bruce H. Mock,[2] Qi-Huang Zheng,[2] Sunil Badve,[3] Gary D. Hutchins,[2] and George W. Sledge, Jr.[1]

Abstract

Background: This pilot study combined physiologic imaging, microcomputed tomography, and histologic tumor evaluation with a xenograft model of breast cancer to identify surrogates likely to correlate with response to AZD2171, an inhibitor of the vascular endothelial growth factor (VEGF) receptor tyrosine kinases.

Experimental Design: MCF-7 cells transfected with vector (MCF-7^{neo}) or VEGF (MCF^{VEGF}) were implanted in the right and left mammary fat pads of 75 athymic mice. Treatment with AZD2171 (5 mg/kg/d) or vehicle control was initiated once tumors were established. Positron emission tomography with [^{11}C]carbon monoxide to measure blood volume, [^{18}F]fluoromethane to measure perfusion, and [^{18}F]fluorodeoxyglucose to measure glucose utilization was done at baseline, and after 24 hours, 72 hours, and 4 weeks of treatment. After imaging, tumors were analyzed for microvessel density, proliferation, and VEGF expression.

Results: AZD2171 induced significant inhibition of tumor growth in established MCF-7^{neo} xenografts and regression of established MCF-7^{VEGF} xenografts. An acute decrease in blood flow was detected in MCF-7^{VEGF} tumors at 24 hours ($P = 0.05$). Tumor blood volume was increased in the MCF-7^{VEGF} tumors but correlated with tumor size; blood volume did not change with AZD2171 therapy. Glucose utilization correlated with tumor size and did not change with acute or chronic AZD2171 therapy. Unlike blood flow and blood volume, glucose utilization was similar in MCF-7^{neo} and MCF-7^{VEGF} tumors. Microvessel density and proliferation acutely decreased in MCF-7^{VEGF} tumors but returned to baseline during chronic therapy.

Conclusions: [^{18}F]Fluoromethane imaging may be a useful surrogate for biological activity of AZD2171 with changes identified within 24 hours of starting therapy.

Over the last two decades, substantial laboratory and indirect clinical evidence has accumulated to support the central role of angiogenesis in breast cancer progression (1, 2). Multiple angiogenic factors are commonly expressed by invasive human breast cancers with the 121-amino-acid isoform of vascular endothelial growth factor (VEGF) predominating (3). VEGF is a highly conserved, homodimeric, secreted, heparin-binding glycoprotein whose dominant isoform has a molecular weight of ~45,000 (4). The biological effects of VEGF are mediated through binding to one of three endothelial surface receptors VEGF receptor-1 (VEGFR-1, Flt-1), VEGFR-2 (Flk-1/KDR), and VEGFR-3 (Flt-4); binding to the coreceptor neuropilin enhances signaling (5, 6). The VEGFRs share considerable overlap in ligand binding, downstream effector interaction, and biological function; however, predominant actions have been identified for each. VEGFR-1 promotes differentiation and vascular maintenance (7); VEGFR-2 induces endothelial cell mitogenesis, survival, and migration and increases vascular permeability (8); VEGFR-3 stimulates lymphangiogenesis (9, 10).

AZD2171, a novel indole-ether quinazoline, is a highly potent (IC_{50} < 1 nmol/L) inhibitor of the VEGFR-2 tyrosine kinase. AZD2171 inhibits VEGF-stimulated endothelial cell proliferation and *in vitro* vessel growth and sprotting. *In vivo* AZD2171 inhibits experimental angiogenesis, endochondral ossification, and growth of established human tumor xenografts in a dose-dependent fashion (11). Early clinical trials with AZD2171 in patients with advanced cancer are ongoing (12, 13).

Correlative laboratory studies assessing biologically meaningful intermediate end points are a necessity for the successful development of antiangiogenic therapy. Although, as yet, no clear standard has emerged, the search for reliable surrogates of antiangiogenic activity has focused on two main areas: soluble factors and imaging the tumor vasculature. This pilot study combines functional and anatomic imaging using small animal

Authors' Affiliations: [1]Division of Hematology and Oncology, Department of Medicine; [2]Division of Imaging Sciences, Department of Radiology; and [3]Department of Pathology, Indiana University, Indianapolis, Indiana

Received 1/31/05; revised 9/1/05; accepted 9/15/05.

Grant support: Breast Cancer Research Foundation (G.W. Sledge and K.D. Miller), Walther Medical Foundation (G.W. Sledge), National Cancer Institute grant P20-CA86350 (G.D. Hutchins), Indiana Genomics Initiative (supported in part by the Lilly Endowment; G.D. Hutchins), and an unrestricted research grant from AstraZeneca (K.D. Miller).

The costs of publication of this article were defrayed in part by the payment of page charges. This article must therefore be hereby marked *advertisement* in accordance with 18 U.S.C. Section 1734 solely to indicate this fact.

Requests for reprints: Kathy D. Miller, Division of Hematology and Oncology, Indiana University, Indiana Cancer Pavilion, 535 Barnhill Drive, RT-473, Indianapolis, IN 46202. Phone: 317-274-0920; Fax: 317-274-3646; E-mail: kathmill@iupui.edu.

doi:10.1158/1078-0432.CCR-05-0219

positron emission tomography (PET) and microcomputed tomography (micro-CT) techniques in a xenograft model of breast cancer to identify PET tracers likely to correlate with response to AZD2171. Tumor growth and imaging were compared with histologic changes in tumor vascularity, proliferation, and VEGF expression.

Materials and Methods

Orthotopic xenograft model

Six- to eight-week-old female athymic (*nu/nu*) mice (n = 75) were purchased from Harlan Sprague-Dawley (Indianapolis, IN) and acclimated for 7 to 10 days. As MCF-7 tumor cells require supplemental estrogen for growth in athymic mice, a controlled release estradiol pellet (0.72 mg, 60-day formulation) was injected s.c. via a sterile 14-gauge trocar at least 24 hours before tumor implantation. Under direct visualization, the right and left mammary fat pads were injected with 5×10^6 MCF-7^{neo} (non-VEGF expressing) or 1×10^6 MCF-7^{VEGF} (VEGF expressing) cells in 0.1 mL of Hanks' buffered saline (14, 15). This dual implantation technique allowed comparison of physiologic imaging, tumor growth, and response to AZD2171 in tumors with high and low levels of VEGF production within the same animal. In preliminary studies, this dual implantation technique did not alter tumor growth or vascularity compared with tumors implanted singly (data not shown).

Once tumors were established (~5-8 mm diameter), mice were divided into five groups; baseline imaging (n = 15), imaging 24 hours after a single dose of AZD2171 (n = 15), imaging 72 hours after initiation of AZD2171 treatment (n = 15), and imaging after 4 weeks of treatment with either AZD2171 (n = 15) or vehicle control (n = 15). AZD2171 (5 mg/kg/d) or vehicle (100 μL) was administered by oral gavage once daily, starting on day 20 after implantation. A single observer (K.D. Miller) measured tumor diameter in two dimensions with vernier calipers twice weekly throughout treatment; tumor volume was calculated as 3.14 / 6 × largest diameter × smallest diameter squared. All animal experiments were done under a protocol approved by the Indiana University Institutional Animal Care and Use Committee.

Positron emission tomography imaging

PET imaging was done to measure tumor blood volume with [^{11}C]carbon monoxide ([^{11}C]CO; refs. 16, 17), perfusion with [^{18}F]fluoromethane ([^{18}F]FCH_3; refs. 18, 19), and glucose utilization with [^{18}F]fluorodeoxyglucose ([^{18}F]FDG). Studies were done using the IndyPET-II scanner (20) using 120 CTI HR detector modules arranged in four detector banks. The detector banks are arranged to produce a transaxial field of view of 23 cm and an axial field of view of 15 cm. Within an axial plane, the average full-width-at-half-maximum resolution is 2.5 mm at the center of the field of view with minimal resolution degradation over the central 10 cm of the field of view (20). The NEMA-2001 sensitivity is 9,030 cps/MBq at the center of the scanner and 4,250 cps/MBq at a distance of 10 cm from the center of the field of view. All data are acquired with a 350 to 650 keV energy window. The IndyPET-II scanner collects all data in list mode (the time and location of individual events is recorded). Following data acquisition, events are combined to form event versus position histograms (sinogram) used for image reconstruction. List mode data acquisition enables the retrospective formation of sinogram data over discrete time intervals for tracer kinetic analysis.

Radiotracers. [^{11}C]CO was produced via the $^{14}N(p,\alpha)^{11}C$ nuclear reaction starting from research grade natural nitrogen gas using the RDS-112 cyclotron (CTI, Inc., Knoxville, TN). Following irradiation at 40 μA for 20 minutes, the in-target [^{11}C]CO and [^{11}C]CO_2 target gas mixture was exhausted through a 950°C charcoal furnace for complete conversion to [^{11}C]CO. Typical production yielded >500 mCi of product in ~250 mL of nitrogen carrier gas collected in the gas bag at end of bombardment. Ten-milliliter aliquots containing ~20 mCi of [^{11}C]CO were delivered to the animal scanner facility for unit-dose preparation and administration.

[^{18}F]FCH_3 was prepared using the method of Gatley et al. (21). Briefly, aqueous [^{18}F]fluoride, produced by the $^{18}O(p,n)^{15}F$ nuclear reaction starting from oxygen-18–enriched water, was azeotroped to dryness with acetonitrile in the presence of 10 mg Kryptofix 2.2.2, 2 mg K_2CO_3, and ~20 mg Ag_2O. Upon addition of 0.1 mL CH_3I and 0.5 mL acetonitrile, [^{18}F]FCH_3 was liberated and swept from the reaction vial with nitrogen gas. Flow was diverted through a water-ice bath and a C_{18} Sep-Pak cartridge to reduce the amount of carrier CH_3I and acetonitrile collected in the gas bag. Typical production yielded >300 mCi of [^{18}F]FCH_3 in 100 mL of nitrogen carrier gas in the gas bag at end of bombardment. Ten-milliliter aliquots containing ~30 mCi of product were delivered for unit-dose preparation and administration.

[^{18}F]FDG was prepared by the Hamacher method using a commercial synthesis unit provided by PETNET/CTI (22).

Gas tracer administration. An in-house gas administration system was developed for the [^{11}C]CO and [^{18}F]FCH_3 studies (Fig. 1A). The mouse is positioned on the scanning bed with a mask surrounding the entire head. The mask, made from a 60 mL syringe, is cylindrical, ~25 mm in diameter, and 50 mm in length with a total internal volume of ~25 mL. A latex membrane with a central hole, through which the head of the mouse is inserted, covers the open end of the mask. This membrane provides a seal around the neck of the mouse while still being loose enough that it does not constrict blood flow or respiration. The mask has two female leur fittings. The first leur fitting is at the end of the syringe and the second is mounted in the side of the syringe. The side fitting is attached to a stopcock and a small air pump. The gas tracer

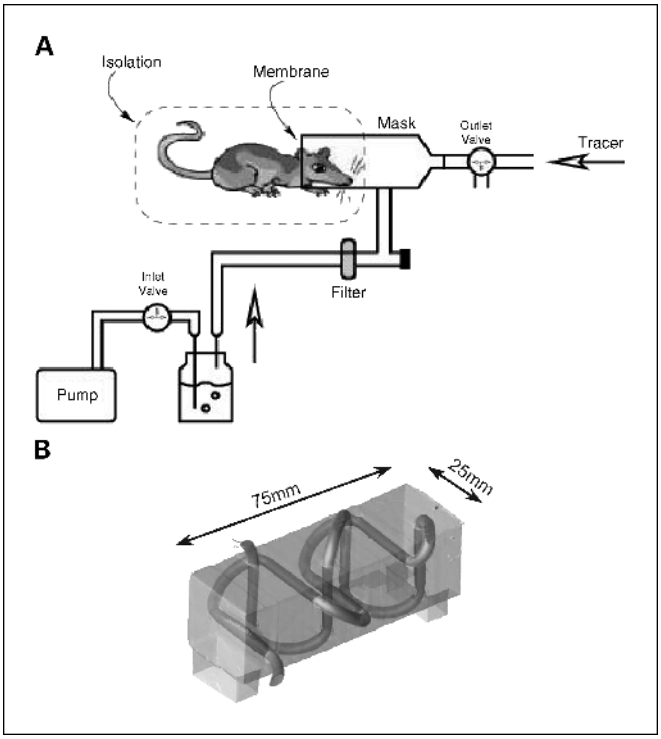

Fig. 1. The apparatus for delivery of gaseous tracers (*A*) and image registration (*B*). *A,* the mouse is positioned on the scanning bed with a mask surrounding the entire head. A latex membrane with a central hole through which the head of the mouse is inserted covers the open end of the mask. Two female leur fittings allow connection to an air pump with separate administration of gaseous tracers. *B,* PET-CTregistration phantom consists of parallel and perpendicular tubes filled with a mixture of [^{18}F]FDG and iodinated contrast agent. Imaging stages for both the EVS RS-9 micro-CTand IndyPET-II have identical mounts with precision pins that ensure reproducible positioning. Transformation variables are calculated using an algorithm that finds the ends of the tubes and calculates a geometric transform using the locations of the end points in the two image pairs.

is prepared by loading ~37 MBq (~1 mCi) of tracer in 1 to 2 mL into a 3 mL syringe. This syringe is coupled to the end of the mask with a stopcock. After starting image acquisition, the stopcock to the air pump is closed and the gas tracer is introduced into the mask. The mouse is allowed to rebreathe the tracer for 2 minutes. After this uptake period, the stopcocks are opened to allow the air pump to circulate ~100 mL of room air through the mask and out the end, flushing the remaining tracer out of the mask.

[^{18}F]Fluorodeoxyglucose administration. [^{18}F]FDG (1 mCi) was administered i.v. to the mouse via tail vein.

Imaging protocol. Before each imaging session, anesthesia was administered to the animals in a laminar flow hood. Once anesthetized with ketamine, animals were placed in a small isolation chamber for the imaging procedures. The isolation chamber is integrated with the gas administration system previously described to isolate each animal from the external environment. Each animal imaging session began with a high resolution X-ray CT scan using the EVS MS-9 scanner (Enhanced Vision Systems Corp., London, Ontario, Canada) in the 100 μm voxel resolution mode. Images were reconstructed using a Feldcamp cone beam reconstruction algorithm. The CT image data serves as an anatomic reference to aid interpretation of the PET image data and is used to generate attenuation correction information to reconstruct quantitative images of radionuclide concentrations. PET data is acquired in list mode for 30 minutes and sorted into 17 × 20–second frames, 4 × 60–second frames, and 4 × 300–second frames after the acquisition is complete. Frames are reconstructed with an 80 mm transaxial field of view, 0.625 mm pixels, and 47 slices spaced 3.15 mm apart. Reconstruction is done with filtered back-projection using a Hanning filter with a cutoff frequency of 4.2/cm.

Image registration and fusion. We have developed a method for registering small animal scans acquired with the IndyPET-II PET scanner and the EVS RS-9 micro-CT scanner. After sedation, the subject is strapped to a scanning bed (previously described), which is mounted on the EVS micro-CT imaging stage for CT image acquisition. Following the CT scan, the bed is moved from the EVS micro-CT stage to the IndyPET II imaging stage. Both stages have identical mounts with precision pins so that the bed position is reproducible. A six-variable rigid body registration transform of the PET image to the CT image space is calculated using PET and CT images of a registration phantom consisting of parallel and perpendicular tubes filled with a mixture of [^{18}F]FDG and iodinated contrast agent. A CT image of the registration phantom is shown in Fig. 1B. Transformation variables were calculated using an algorithm that finds the ends of the tubes and calculates a geometric transform using the locations of the end points in the two image pairs. This method also provides a measure of fiducial registration error. Typically, the overall fiducial registration error is <0.4 mm. The phantom-derived registration transformation variables were applied to the animal CT and PET data sets to register the anatomic and functional image data sets for further evaluation.

Positron emission tomography data analysis

PET and CT images are registered and regions of interest are drawn on the tumors, thigh muscle, heart blood pool, and the left and right lungs using the CT image to identify the tumor and tissue regions. For the [^{18}F]FCH_3 studies, time-activity curves are calculated by applying the regions of interest to each frame of the PET image.

Blood volume estimates. The [^{11}C]CO tracer tightly binds to RBC following administration and provides an image of RBC distribution in tissue. Fractional blood volume estimates are obtained by taking the ratio of [^{11}C]CO concentration in a tissue region of interest [$C_t(t)$] to the [^{11}C]CO concentration in a blood volume region of interest [left ventricular chamber of the heart; $C_a(t)$]. To reduce statistical uncertainty, the blood volume fraction (BVF) estimate image data is integrated over a period of 10 minutes following equilibration of the [^{11}C]CO throughout the blood pool. A period of 5 minutes following tracer administration is used to assure equilibration of [^{11}C]CO within the vascular spaces before integration of the tissue and blood pool signal. BVF estimates were calculated using Eq. A.

$$\mathrm{BVF} = \frac{\int_5^{15} C_t(t)\mathrm{d}t}{\int_5^{15} C_a(t)\mathrm{d}t} \quad \text{(A)}$$

Estimates of tumor blood volume were calculated by multiplying BVF by the physical tumor volume (V_T) obtained by placing regions of interest on the X-ray CT images.

$$\mathrm{BF} = \mathrm{BVF}xV_T \quad \text{(B)}$$

Perfusion estimates. A one-compartment tracer kinetic model is fit to the tissue-activity curves using the lung curves as the input function. This model fits Eq. C to the measured tissue curve $C_t(t)$. This model is the Kety-Schmidt single-compartment model for diffusible tracers (23, 24) with an additional term added to account for tracer in the vascular compartment.

$$C_t(t) = (1 - \mathrm{BVF}) \int_{t_1}^{t_2} K_1 C_a(t) \otimes e^{-K_1/V_d t}\mathrm{d}t + \mathrm{BVF} \int_{t_1}^{t_2} C_a(t)\mathrm{d}t \quad \text{(C)}$$

The variables of the fit are K_1, V_d, and BVF, which are related to the traditional blood flow (perfusion) variable, distribution volume, and BVF. The applicability of this model follows from our assumption that the tracer concentration in the lungs is in equilibrium with the tracer concentration in the blood. The unknown ratio of blood to lung activity concentration is folded into the blood volume variable BVF.

Total blood flow (TBF) through the tumor was calculated by using Eq. D.

$$\mathrm{TBF} = K_1 V_t \quad \text{(D)}$$

Fluorodeoxyglucose utilization estimates. FDG uptake estimates are generated by placing regions of interest on PET images acquired over the time period from 45 to 60 minutes after tracer administration. This imaging time window was selected to enable sufficient clearance of nonmetabolized FDG from the tissue to provide an image that is dominated by tracer that has been phosphorylated by hexokinase and trapped in the tissue. Indices of tumor FDG uptake were generated by calculating the total FDG uptake in the tumor normalized by the mass of the animal and the injected dose of tracer. Eq. E was used to generate FDG uptake indices ($\mathrm{UI_{FDG}}$). $\mathrm{UI_{FDG}}$ is the fraction of the injected dose in the tumor ($\mathrm{FID_T}$) normalized by the mass of the animal.

$$\mathrm{UI_{FDG}} = \frac{V_T \int_{45}^{60} C_t(t)\mathrm{d}t}{20(60-45)(M/D)} = \frac{\mathrm{FID_T}M}{20} = \frac{V_T \mathrm{SUV}}{20} \quad \text{(E)}$$

In Eq. E, V_t is the tumor volume derived from the CT images, $C_t(t)$ is the PET measured tracer uptake in the tumor, M is the mass of the animal, and D is the injected dose of FDG. The ratio of $M/20$ in this equation is to normalize the fraction of the injected dose to a standard 20 g mouse. The $\mathrm{UI_{FDG}}$, therefore, represents the fraction of the injected dose that accumulates in the tumor for a standard 20 g mouse. In Eq. E, SUV is the standardized uptake value normally used in clinical PET studies.

Histology

Primary tumors were resected after imaging and fixed in 10% buffered neutral formalin for subsequent histologic analysis of microvessel density (CD31), proliferation (Ki-67), and VEGF expression. Tumors after 4 weeks of treatment with AZD2171 or control frequently had necrotic centers; only viable tumor was processed for analysis.

Microvessel density

Specimens were dewaxed in xylene and rehydrated through descending grades of alcohol. Antigen retrieval was done in DAKO citrate buffer (pH 6; DAKO, Carpinteria, CA) for 20 minutes in a 95°C water bath. Endogenous peroxidase activity was blocked using 3% hydrogen peroxide. Endogenous biotin and avidin was blocked using DAKO avidin/biotin each for 10 minutes; nonspecific binding was minimized using a protein block for 20 minutes. Slides were then incubated for 30 minutes with DAKO prediluted mouse monoclonal CD31 then followed by sequential application of DAKO-LSAB2 biotinylated link antibody and DAKO-LSAB2 streptavidin labeled with alkaline phosphatase for 15 minutes each. 3,3′-Diaminobenzidine tetrahydrochloride was used as the chromogen for visualization; sections were counterstained with hematoxylin QS, dehydrated through ascending grades of alcohol, cleared in xylene, and mounted.

Microvessel density was counted using previously published methods (25–27). The tumor periphery was scanned at low power to identify the three areas of greatest vessel density. These areas were then examined under high power (0.7386 mm^2 per 200× field). Any brown staining endothelial cell or cell cluster clearly separated from adjacent microvessels was counted. A vessel lumen or the presence of red cells was not required; microvessels with a diameter >50 μm were excluded. Both the maximum and average of all three fields were reported.

Proliferation

Sections were dewaxed in xylene and rehydrated through descending grades of alcohol. Antigen retrieval was done in DAKO Target Retrieval for 20 minutes in a 95°C water bath. Endogenous biotin and avidin was blocked using DAKO avidin/biotin each for 10 minutes. Endogenous peroxidase activity was blocked using 3% hydrogen peroxide. The slides were incubated for 30 minutes with DAKO mouse monoclonal Ki-67 (MiB-1) at a dilution of 1:60, followed by sequential application of DAKO-LSAB2 biotinylated link antibody and DAKO-LSAB2 streptavidin labeled with alkaline phosphatase for 15 minutes each. 3,3′-Diaminobenzidine tetrahydrochloride was used as the chromogen for visualization; sections were counterstained with hematoxylin QS, dehydrated through ascending grades of alcohol, cleared in xylene, and mounted. The Ki-67 labeling index was determined by counting the number of positive nuclei in 1,000 tumor cells in at least five representative high-power fields (×400) with selection of fields that contained viable tumor cells (28).

Vascular endothelial growth factor expression

Sections were dewaxed in xylene and rehydrated through descending grades of alcohol; slides were rinsed between grades with TBS. Antigen retrieval was done in DAKO Target Retrieval for 20 minutes in a 95°C water bath. Endogenous biotin and avidin was blocked using DAKO avidin/biotin each for 10 minutes. Endogenous peroxidase activity was blocked using 3% hydrogen peroxide. Nonspecific binding of antibody was minimized using a protein block for 20 minutes; excess protein block was tapped off the slides without rinsing. Slides were incubated for 1 hour with Biogenix (Bogota, Columbia) prediluted rabbit polyclonal VEGF diluting it further in a 1:2 ratio, followed by sequential application of DAKO-LSAB2 biotinylated link antibody and DAKO-LSAB2 streptavidin labeled with alkaline phosphatase for 15 minutes each. 3,3′-Diaminobenzidine tetrahydrochloride was used as the chromogen; sections were counterstained with hematoxylin QS. Slides were dehydrated through ascending grades of alcohol followed by clearing in xylene and mounted. VEGF expression was reported using the following scoring system: 0, negative; 1, weak staining in <10% of tumor cells; 2, moderate or high intensity staining in >10% of tumor cells. At least five representative high-power fields (×400) containing viable tumor cells were evaluated.

Statistical analyses

All statistical analyses were done using Student's t test. $P < 0.05$ denoted the presence of a statistically significant difference. In previous studies, we found no acute alteration in any of the PET or histologic variables with vehicle control. To limit the number of animals required, acute time points (24 and 72 hours) were compared with baseline studies; tumor size was comparable in these groups. *In vivo* tumor growth analyses were done using GraphPad Prism version 3.02 for Windows (GraphPad Software, San Diego, CA; www.graphpad.com).

Results

Inhibition of* in vivo *tumor growth. As expected, MCF-7^{VEGF} xenografts grew more rapidly and formed larger tumors than MCF-7^{neo} xenografts in the absence of active treatment. Chronic once-daily oral administration of AZD2171 (5 mg/kg) induced a statistically significant (P = 0.027) regression of established MCF-7^{VEGF} xenografts (Fig. 2). In contrast, AZD2171 treatment did not induce regression, but inhibited the growth of MCF-7^{neo} tumors, although this did not reach statistical significance using a Kaplan-Meier–based analysis.

Tumor histology. MCF-7^{VEGF} tumors were more vascular (P = 0.0001) and had a higher proliferative fraction (P = 0.002) than MCF-7^{neo} tumors at baseline. An acute decrease in tumor microvessel density was apparent 24 hours after treatment with AZD2171 in MCF-7^{VEGF} tumors (P = 0.057) with an even more pronounced decrease at 72 hours (P = 0.0003). Despite continued control of tumor growth, MCF-7^{VEGF} tumors exposed to chronic daily AZD2171 therapy for 4 weeks had a microvessel density similar to MCF-7^{VEGF} tumors treated with vehicle alone. Similarly, proliferation as measured by Ki-67 index acutely decreased in MCF-7^{VEGF} tumors (P = 0.036 at 24 hours and P = 0.0016 at 72 hours) but returned to baseline during chronic therapy. In contrast, no significant difference in tumor microvessel density or proliferation was seen in MCF-7^{neo} tumors after either acute or chronic exposure to

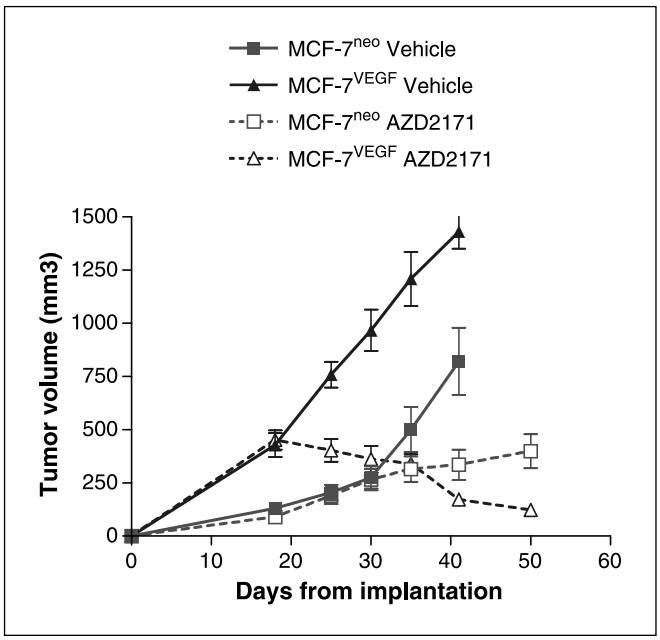

Fig. 2. Impact of chronic AZD2171 treatment on tumor growth *in vivo.* MCF-7^{neo} (5×10^6) and MCF7^{VEGF} (1×10^6) cells in 0.1 mL of Hanks' buffered saline were injected into the right and left mammary fat pads, respectively, of athymic mice. Supplemental estradiol was provided by a controlled release s.c. pellet. AZD2171, 5 mg/kg/d, or vehicle control was administered by oral gavage starting on day 19. Tumors were measured with calipers twice weekly throughout treatment. Points, mean; bars, SE.

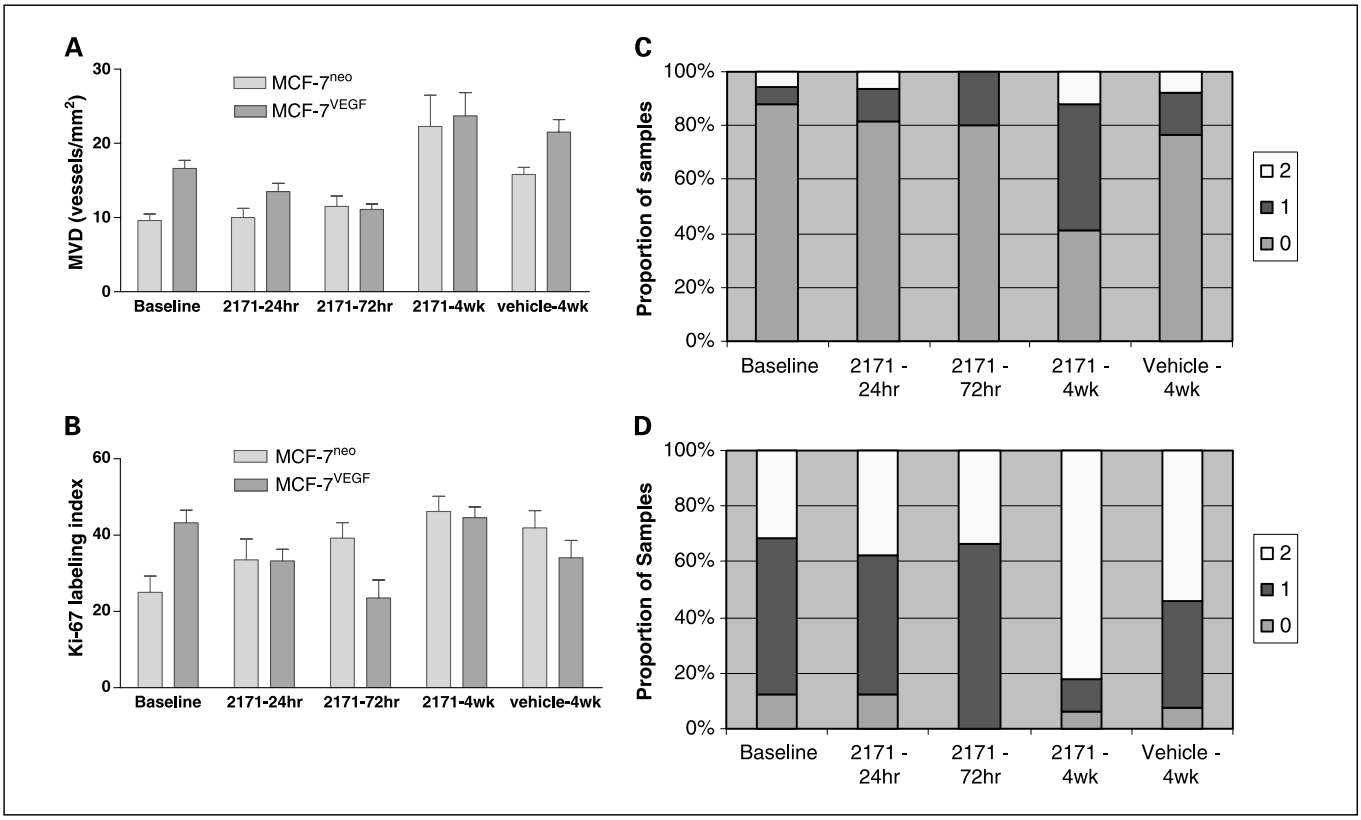

Fig. 3. Impact of AZD2171 on tumor vascularity (*A*), proliferation (*B*), and VEGF expression (*C* and *D*). *A,* microvessel density (*MVD*) is acutely decreased in MCF-7^{VEGF} tumors ($P = 0.057$ at 24 hours and $P = 0.0003$ at 72 hours) by AZD2171 but returns to baseline levels during chronic therapy. Tumors were stained with mouse monoclonal CD31 antibody. The average microvessel density of all three fields is reported; analysis of maximum microvessel density yielded similar results (data not shown). *B,* proliferation is acutely decreased in MCF-7^{VEGF} tumors ($P = 0.036$ at 24 hours and $P = 0.0016$ at 72 hours) but returned to baseline during chronic therapy. Tumors were stained with mouse monoclonal Ki-67 (MiB-1) antibody; the number of positive nuclei in 1,000 tumor cells is reported. Columns, mean; bars, SE. *C,* chronic, but not acute, therapy with AZD2171 increases VEGF expression in MCF-7^{neo} tumors ($P = 0.02$). *D,* no change in VEGF expression is seen in MCF-7^{VEGF} tumors after 24 or 72 hours of AZD2171 therapy. In contrast, VEGF expression significantly increases after 4 weeks of AZD2171 therapy ($P = 0.01$). Tumors were stained with rabbit polyclonal VEGF antibody. VEGF expression was reported as follows: 0, negative; 1, weak staining in <10% of tumor cells; 2, moderate or high-intensity staining in ≥10% of tumor cells.

AZD2171 (Fig. 3). As anticipated, a higher VEGF expression was detected in the MCF-7^{VEGF} tumor compared with the MCF-7^{neo} tumors. No acute change in VEGF expression was detected with AZD2171 therapy; however, chronic therapy with AZD2171 increased VEGF expression in both MCF-7^{neo} and MCF-7^{VEGF} tumors ($P = 0.02$ and $P = 0.01$, respectively; Fig. 3).

Physiologic imaging. Perfusion (tissue blood flow) is increased >20-fold and is more variable in MCF-7^{VEGF} compared with MCF-7^{neo} tumors (Fig. 4A). An acute decrease in perfusion is apparent in MCF-7^{VEGF} tumors 24 hours after starting AZD2171 therapy ($P = 0.05$). Perfusion is more dramatically decreased after 72 hours of AZD2171 treatment ($P = 0.03$). Perfusion in MCF-7^{neo} tumors is similar to that of normal muscle and is not altered by AZD2171. [^{18}F]FCH_3 volume of distribution is not altered by treatment with AZD2171 (Fig. 4B). Total tumor blood flow does not correspond with tumor volume, confirming that the treatment-induced perfusion changes are not due to differences in tumor size (Fig. 4C).

Although we detected a statistically significant decrease in blood volume in MCF-7^{VEGF} tumors 24 hours after AZD2171 therapy by [^{11}C]CO (data not shown), no difference was seen at 72 hours or after 4 weeks of therapy. Importantly, we observed a consistent relationship between total tumor blood volume and tumor volume independent of treatment in MCF-7^{VEGF} tumors (Fig. 5A). Tumor-associated blood volume was increased 3-fold in MCF-7^{VEGF} compared with MCF-7^{neo} tumors (data not shown); no consistent change with treatment was identified in either xenograft model (Fig. 5B).

Glucose utilization, as estimated by the [^{18}F]FDG uptake index, was associated with tumor size and did not change with acute or chronic AZD2171 therapy in MCF-7^{VEGF} tumors (data not shown). Unlike blood flow and blood volume, glucose utilization was similar in MCF-7^{neo} and MCF-7^{VEGF} tumors (Fig. 6).

Discussion

We developed a breast cancer xenograft model system allowing direct comparison of tumor response, histology, and physiologic imaging based on VEGF expression. Dual implantation of controls and VEGF-transfected MCF-7 cells allows each animal to serve as its own control, decreasing both the variability and number of animals required. As expected, MCF-7^{VEGF} tumors were more vascular than MCF-7^{neo} tumors (14). The increased microvessel density seen with MCF-7^{VEGF} tumors was associated with an increase in proliferation as measured by Ki-67. The increase in tumor growth, microvessel density, proliferation, and perfusion confirm that VEGF secreted from the MCF-7^{VEGF} xenograft had little effect on the MCF-7^{neo} xenograft in the contralateral fat pad. Using this model, we have shown that the

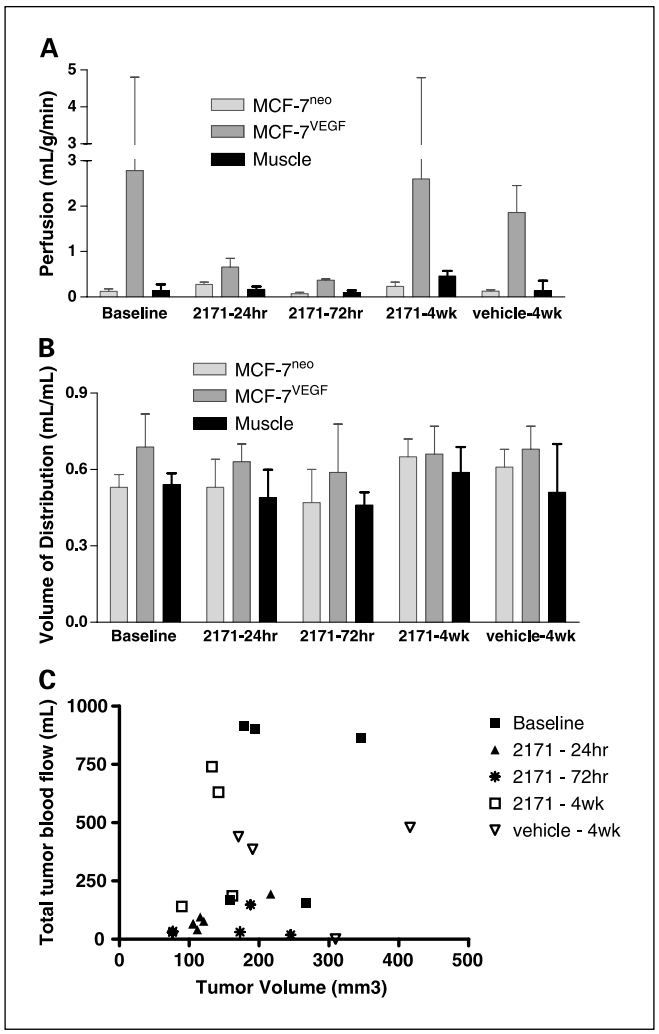

Fig. 4. Tumor perfusion as measured by [^{18}F]FCH_3. *A,* AZD2171 acutely decreases perfusion in MCF-7^{VEGF} tumors ($P = 0.05$ at 24 hours and $P = 0.03$ at 72 hours). Perfusion in MCF-7^{neo} tumors is similar to that of normal muscle and is not altered by AZD2171. *B,* [^{18}F]FCH_3 volume of distribution is not altered by treatment with AZD2171. *C,* total tumor blood flow does not correlate with tumor volume in MCF-7^{VEGF} tumors (or in MCF-7^{neo} tumors; data not shown). Columns (*A* and *B*), mean; bars, SE.

effect of the small-molecule VEGFR-2 tyrosine kinase inhibitor AZD2171 on tumor growth is at least partially dependent on VEGF expression. MCF-7^{neo} tumors remained growth inhibited, whereas VEGF-expressing MCF-7^{VEGF} significantly regressed.

Physiologic imaging using the IndyPET-II system was able to distinguish VEGF and non-VEGF-expressing tumors within a single animal. Interestingly, blood volume and perfusion of the non-VEGF-expressing MCF-7^{neo} tumors was similar to normal skeletal muscle in this model. Although PET imaging of tumor perfusion and/or blood volume has been incorporated into early clinical trials (18, 29, 30), few studies have compared perfusion in tumor and normal tissue. Wells et al. (31) found that [^{15}O]CO_2 PET measurements of regional blood flow are reproducible in patients with predominantly intra-abdominal malignancies but did not compare perfusion to normal tissues. In one study of eight patients with simultaneous parallel measurements, renal tumor perfusion was significantly lower than perfusion of the normal kidney (32).

Treatment with AZD2171 induces an acute decrease in tumor perfusion in MCF-7^{VEGF} tumors that can be detected within 24 hours; a further decrease was detected at 72 hours. Histologic analysis of viable tissue from treated tumors found decreases in tumor microvessel density and proliferation in a time course that paralleled the decrease in perfusion. Although tumor blood volume was increased in the MCF-7^{VEGF} tumors, blood volume was not altered by AZD2171 therapy. The tumor blood volume measured by PET represents blood in both large and small vessels within the tumor. The inability to detect blood volume changes using PET in the setting of observed changes in microvessel density by histology suggests that small vessels, easily quantified by histology, are most affected by AZD2171 but carry only a small fraction of the total tumor blood volume.

Compensatory mechanisms, as yet not fully defined, restore perfusion during 4 weeks of continuous daily therapy in our model. We detected an increase in VEGF expression in both MCF-7^{neo} tumors and MCF-7^{VEGF} tumors exposed to chronic AZD2171 therapy. Inhibition of VEGF signaling by AZD2171 could induce tumor hypoxia, with a resultant increase in VEGF expression. Other potential compensatory mechanisms, not investigated in this study, include induction of other proangiogenic peptides, mutation of the VEGFR tyrosine kinase, or co-option of existing host vessels. As our study did not include pharmacokinetic assessments, we cannot exclude increased clearance or altered distribution of AZD2171 during chronic

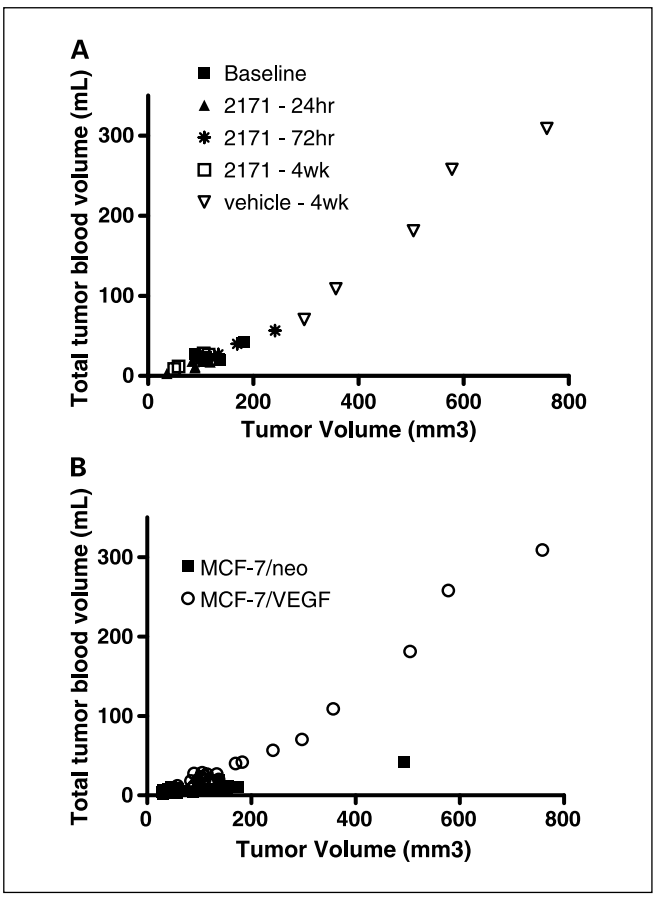

Fig. 5. Tumor blood volume as measured by [^{11}C]CO. *A,* total tumor blood volume correlates with tumor volume and is independent of treatment in MCF-7^{VEGF} and MCF-7^{neo} tumors (data not shown). *B,* tumor-associated blood volume was increased 3-fold in MCF-7^{VEGF} compared with MCF-7^{neo} tumors.

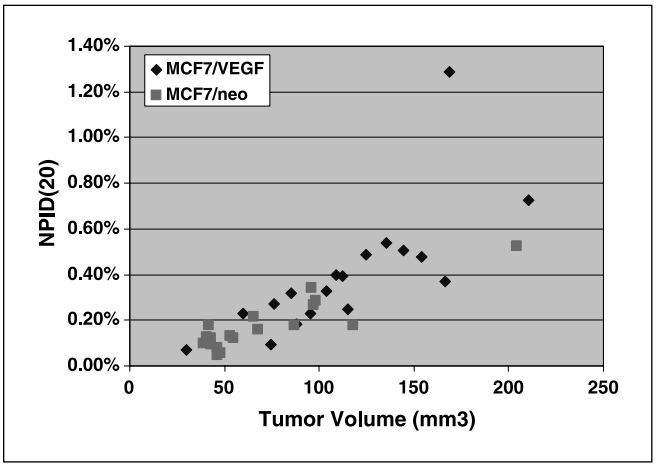

Fig. 6. Tumor glucose utilization as measured by [^{18}F] FDG. Glucose utilization was similar in MCF-7^{neo} and MCF-7^{VEGF} tumors and does not change with acute or chronic AZD2171 therapy. The percentage of the administered FDG that accumulated in the tumor normalized to a reference animal weight of 20 g [*NPIG(20)*, percentage of FDG uptake in tumor expected if individual animals weighed 20 g] is plotted versus tumor volume. The close correspondence of each curve serves as an indicator that the FDG uptake per unit volume or cell within the tumor (slope of curves) is unchanged between groups and following AZD2171 therapy.

therapy although this has not been observed previously in other studies.[4]

The increase in microvessel density we observed during chronic therapy differ from the results reported by Wedge et al. (11) using a s.c. Calu-6 lung cancer xenograft model. Treatment with AZD2171 produced a 47% reduction in vessel number and a 40% reduction in CD31 area after 52 hours; vessel number and CD31 area continued to decrease throughout the 21-day treatment period (≤70% at day 21). Imaging to assess perfusion or blood volume was not done. Critical differences in methodology may account for the difference in results. First, the complex interaction between tumor cells and host microenvironment has been recognized for over a century (33–35). More recently, the effect of the local tumor microenvironment on angiogenesis and response to antiangiogenic therapy has become increasingly clear (36–38). We would expect the tumor microenvironment to affect compensatory mechanisms and the development of resistance as well. Second, Wedge et al. analyzed the entire tumor, normalizing the number of vessels or CD31 area to tumor size. In contrast, we scanned the periphery of the tumor for the area of greatest vascularity. As such, small areas of intense vascularity would have a much greater effect on our results.

Importantly, although perfusion, microvessel density, and proliferation returned to baseline levels during chronic therapy in our study, tumor growth control was maintained. One possible explanation for these seemingly disparate results might be that acute treatment prunes the immature vessels at the tumor periphery leaving the mature vessels in the center of the tumor (39). These mature, normal vessels would support persistence of a residual smaller, but well-vascularized, tumor with proliferation matched by apoptosis (40, 41). Unfortunately, we were unable to assess apoptosis to investigate this hypothesis. Alternatively, overt resistance and tumor growth may have ensued quickly with further therapy, although resistance to VEGFR tyrosine kinase inhibitors (including AZD2171) has not been documented previously in tumor xenograft models (11, 42, 43).

In our study, total [^{18}F]FDG uptake correlated only with tumor size; no association was found with VEGF expression, [^{18}F]FCH_3, or [^{11}C]CO uptake or AZD2171 treatment. Tumor glucose utilization is tightly controlled. Consequently, FDG uptake is complex and may be affected by many factors besides perfusion and blood volume (44, 45). Two small studies found a correlation with [^{18}F]FDG uptake and tumor blood flow as assessed by [^{15}O]H_2O in primary breast cancers (46–48). Nonetheless, our results suggest that [^{18}F]FDG imaging is not a reliable surrogate for changes in tumor vasculature and activity of antiangiogenic agents.

Using this model, we previously showed a dose-dependent decrease in tumor blood volume and perfusion after 4 weeks of treatment with ZD6474, an inhibitor of the VEGFR-2 and epidermal growth factor tyrosine kinases; the acute effects of ZD6474 therapy were not imaged (49). In contrast, our results differ from studies using another VEGFR tyrosine kinase inhibitor in this model. Whereas AZD2171 had little effect on tumor blood volume, SU11248 treatment induced an acute decrease in tumor blood volume that was partially attenuated during chronic therapy. Perfusion increased acutely but decreased throughout chronic SU11248 therapy (50). Although both agents inhibit the VEGFR tyrosine kinases, the spectrum of other kinases they inhibit differs. These results show the need for careful consideration of the biological variable measured when using these imaging techniques as surrogates of antiangiogenic activity. Although the image surrogates used in these studies (blood volume, perfusion, and glucose utilization) are all potentially linked to AZD2171 and SU11248 through modulation of the VEGFR tyrosine kinases, none directly measure kinase inhibition. Consequently, each imaging technique needs to be developed and tested specifically for each agent rather than as a general surrogate for antiangiogenic activity.

The ultimate test of any surrogate marker or imaging technique will come in the clinic. The lack of gold standard and variability of physiologic imaging with different antiangiogenic agents in the same model argues for increased preclinical study. Xenograft models like the one we used here can be used to screen potential imaging techniques, allowing selection of the method most predictive of response to a specific agent for incorporation into clinical trials.

Acknowledgments

We thank Kerry Sanders, Winston Baity, Tanya Martinez, Kristan Boling, and Terry McBride for technical assistance, and Julianne Jürgensmeier and Stephen Wedge for helpful discussions during the design and analysis of this study.

[4] S. Wedge, personal communication.

References

1. Folkman J. What is the evidence that tumors are angiogenesis dependent? J Natl Cancer Inst 1990;82:4–6.
2. Gasparini G. Angiogenesis in breast cancer. Role in biology, tumor progression, and prognosis. In: Bowcock A, editor. Breast cancer: molecular genetics, pathogenesis, and therapeutics. Totowa (NJ): Humana Press Inc.; 1999. p. 347–71.
3. Relf M, LeJeune S, Scott PA, et al. Expression of the angiogenic factors vascular endothelial cell growth factor, acidic and basic fibroblast growth factor, tumor growth factor β-1, platelet-derived endothelial cell

growth factor, placenta growth factor, and pleiotrophin in human primary breast cancer and its relation to angiogenesis. Cancer Res 1997;57:963–9.
4. Ferrara N, Davis-Smyth T. The biology of vascular endothelial growth factor. Endocrinol Rev 1997;18:1–22.
5. Neufeld G, Kessler O, Herzog Y. The interaction of neuropilin-1 and neuropilin-2 with tyrosine-kinase receptors for VEGF. Adv Exp Med Biol 2002;515:81–90.
6. Soker S, Takashima S, Miao HQ, Neufeld G, Klagsbrun M. Neuropilin-1 is expressed by endothelial and tumor cells as an isoform-specific receptor for vascular endothelial growth factor. Cell 1998;92:735–45.
7. Cai J, Ahmad S, Jiang WG, et al. Activation of vascular endothelial growth factor receptor-1 sustains angiogenesis and Bcl-2 expression via the phosphatidylinositol 3-kinase pathway in endothelial cells. Diabetes 2003;52:2959–68.
8. Brekken RA, Overholser JP, Stastny VA, Waltenberger J, Minna JD, Thorpe PE. Selective inhibition of vascular endothelial growth factor (VEGF) receptor 2 (KDR/Flk-1) activity by a monoclonal anti-VEGF antibody blocks tumor growth in mice. Cancer Res 2000;60:5117–24.
9. Skobe M, Hawighorst T, Jackson DG, et al. Induction of tumor lymphangiogenesis by VEGF-C promotes breast cancer metastasis. Nat Med 2001;7:192–8.
10. Kadambi A, Carreira CM, Yun CO, et al. Vascular endothelial growth factor (VEGF)-C differentially affects tumor vascular function and leukocyte recruitment: role of VEGF-receptor 2 and host VEGF-A. Cancer Res 2001;61:2404–8.
11. Wedge SR, Kendrew J, Hennequin LF, et al. AZD2171: a highly potent, orally bioavailable, vascular endothelial growth factor receptor-2 tyrosine kinase inhibitor for the treatment of cancer. Cancer Res 2005;65:4389–400.
12. Drevs J, Medinger M, Mross K, et al. Phase I clinical evaluation of AZD2171, a highly potent VEGF receptor tyrosine kinase inhibitor, in patients with advanced cancer. Proc Am Soc Clin Oncol 2005;23:192s.
13. Ryan C, Stadler W, Roth B, Ouchalski T, Koehler M, Small E. Safety and tolerability of AZD2171, a highly potent VEGF inhibitor, in patients with advanced prostate adenocarcinoma. Proc Am Soc Clin Oncol 2005;23:204s.
14. McLeskey SW, Tobias CA, Vezza PR, Filie AC, Kern FG, Hanfelt J. Tumor growth of FGF or VEGF transfected MCF-7 breast carcinoma cells correlates with density of specific microvessels independent of the transfected angiogenic factor. Am J Pathol 1998;153:1993–2006.
15. Kern FG, McLeskey SW, Zhang L, et al. Transfected MCF-7 cells as a model for breast cancer progression. Breast Cancer Res Treat 1994;31:153–65.
16. Kearfott KJ. Absorbed dose estimates for positron emission tomography (PET): C15O, 15CO, CO15O. J Nucl Med 1982;23:1031–7.
17. Phelps ME, Huang SC, Hoffman EJ, Kuhl DE. Validation of tomographic measurement of cerebral blood volume with C11-labeled carboxyhemoglobin. J Nucl Med 1979;20:328–34.
18. Herholz K, Wagner R, Wienhard K, Heiss WD. Use of ^{18}F-fluoromethane for cerebral blood flow measurement with PET. Nuklearmedizin 1990;29:84.
19. Holden JE, Gatley SJ, Hichwa RD, et al. Cerebral blood flow using PET measurements of fluoromethane kinetics. J Nucl Med 1981;22:1084–8.
20. Rouze N, Hutchins G. Design and characterization of IndyPET-II: a high resolution, high-sensitivity dedicated research scanner. IEEE Trans Nucl Sci 2003;50:1491–7.
21. Gatley SJ, Franceschini R, Ferrieri R, Schyler DJ, Wolf AP. An improved synthesis of the inert, diffusible blood-flow tracer, [^{18}F]fluoromethane. Int J Rad Appl Instrum 1991;42:1049–53.
22. Hamacher K, Coenen H, Stocklin G. Efficient stereospecific synthesis of no-carrier-added 2-[^{18}F]-fluoro-2-deoxy-D-glucose using aminopolyether supported nucleophilic substitution. J Nucl Med 1986;27:235–8.
23. Huang S, Carson R, Phelps M. Measurement of local blood flow and distribution volume with short-lived isotopes: a general input technique. J Cereb Blood Flow Metab 1982;2:99–108.
24. Kety S, Schmidt C. The nitrous oxide method for the quantitative determination of cerebral blood flow in man: theory, procedure, and normal values. J Clin Invest 1948;27:476–83.
25. Tynninen O, Sjostrom J, von Boguslawski K, et al. Tumour microvessel density as predictor of chemotherapy response in breast cancer patients. Br J Cancer 2002;86:1905–8.
26. Weidner N, Folkman J, Pozza F, et al. Tumor angiogenesis: a new significant and independent prognostic indicator in early stage breast carcinoma. J Natl Cancer Inst 1992;84:1875–87.
27. Rubio L, Burgos JS, Morera C, Vera-Sempere FJ. Morphometric study of tumor angiogenesis as a new prognostic factor in nasopharyngeal carcinoma patients. Pathol Oncol Res 2000;6:210–6.
28. Diallo R, Schaefer KL, Bankfalvi A, et al. Secretory carcinoma of the breast: a distinct variant of invasive ductal carcinoma assessed by comparative genomic hybridization and immunohistochemistry. Hum Pathol 2003;34:1299–305.
29. Kurdziel K, Bacharach S, Carrasquillo J, et al. Using PET ^{18}F-FDG, ^{11}CO, and ^{15}O-water for monitoring prostate cancer during a phase II anti-angiogenic drug trial with thalidomide. Clin Positron Imaging 2000;3:144.
30. Logan TF, Jadali F, Egorin MJ, et al. Decreased tumor blood flow as measured by positron emission tomography in cancer patients treated with interleukin-1 and carboplatin on a phase I trial. Cancer Chemother Pharmacol 2002;50:433–44.
31. Wells P, Jones T, Price P. Assessment of inter- and intrapatient variability in C15O2 positron emission tomography measurements of blood flow in patients with intra-abdominal cancers. Clin Cancer Res 2003;9:6350–6.
32. Anderson H, Yap JT, Wells P, et al. Measurement of renal tumour and normal tissue perfusion using positron emission tomography in a phase II clinical trial of razoxane. Br J Cancer 2003;89:262–7.
33. Critical determinants in cancer progression and metastasis. A centennial celebration of Dr. Stephen Paget's "seed and soil" hypothesis. Cancer Metastasis Rev 1989;8:93–197.
34. Viadana E, Au KL. Patterns of metastases in adenocarcinomas of man. An autopsy study of 4,728 cases. J Med 1975;6:1–14.
35. Fidler IJ, Naito S, Pathak S. Orthotopic implantation is essential for the selection, growth and metastasis of human renal cell cancer in nude mice [corrected]. Cancer Metastasis Rev 1990;9:149–65.
36. Gohongi T, Fukumura D, Boucher Y, et al. Tumor-host interactions in the gallbladder suppress distal angiogenesis and tumor growth: involvement of transforming growth factor β1. Nat Med 1999;5:1203–8.
37. Tsuzuki Y, Carreira CM, Bockhorn M, Xu L, Jain RK, Fukumura D. Pancreas microenvironment promotes VEGF expression and tumor growth: novel window models for pancreatic tumor angiogenesis and microcirculation. Lab Invest 2001;81:1439–51.
38. Gohongi T, Todoroki T, Fukumura D, Jain RK. Influence of the site of human gallbladder xenograft (Mz-ChA-1) on angiogenesis at the distant site. Oncol Rep 2004;11:803–7.
39. Jain RK. Normalizing tumor vasculature with anti-angiogenic therapy: a new paradigm for combination therapy. Nat Med 2001;7:987–9.
40. Holmgren L, O'Reilly MS, Folkman J. Dormancy of micrometastases: balanced proliferation and apoptosis in the presence of angiogenesis suppression [see comments]. Nat Med 1995;1:149–53.
41. Jain RK. Normalization of tumor vasculature: an emerging concept in antiangiogenic therapy. Science 2005;307:58–62.
42. Wedge SR, Ogilvie DJ, Dukes M, et al. ZD6474 inhibits vascular endothelial growth factor signaling, angiogenesis, and tumor growth following oral administration. Cancer Res 2002;62:4645–55.
43. Fong TA, Shawver LK, Sun L, et al. SU5416 is a potent and selective inhibitor of the vascular endothelial growth factor receptor (Flk-1/KDR) that inhibits tyrosine kinase catalysis, tumor vascularization, and growth of multiple tumor types. Cancer Res 1999;59:99–106.
44. Avril N, Menzel M, Dose J, et al. Glucose metabolism of breast cancer assessed by ^{18}F-FDG PET: histologic and immunohistochemical tissue analysis. J Nucl Med 2001;42:9–16.
45. Bos R, van Der Hoeven JJ, van Der Wall E, et al. Biologic correlates of (18)fluorodeoxyglucose uptake in human breast cancer measured by positron emission tomography. J Clin Oncol 2002;20:379–87.
46. Zasadny KR, Tatsumi M, Wahl RL. FDG metabolism and uptake versus blood flow in women with untreated primary breast cancers. Eur J Nucl Med Mol Imaging 2003;30:274–80.
47. Mankoff DA, Dunnwald LK, Gralow JR, et al. Blood flow and metabolism in locally advanced breast cancer: relationship to response to therapy. J Nucl Med 2002;43:500–9.
48. Mankoff DA, Dunnwald LK, Gralow JR, et al. Changes in blood flow and metabolism in locally advanced breast cancer treated with neoadjuvant chemotherapy. J Nucl Med 2003;44:1806–14.
49. Miller K, Hutchins G, Miller M, Badve S, Sledge G. ZD6474-mediated vascular changes in a breast cancer xenograft model illustrated by positron emission tomography. AACR-NCI-EORTC Conference, November 19, 2003. Boston, MA.
50. Miller KD, Hutchins GD, Miller M, Badve S, Murray L, Sledge GW. The search for surrogates—physiologic imaging in a breast cancer xenograft model during treatment with SU11248. Breast Cancer Res Treat 2003;77:S18.

Clinical Cancer Research

A Physiologic Imaging Pilot Study of Breast Cancer Treated with AZD2171

Kathy D. Miller, Michael Miller, Sanjana Mehrotra, et al.

Clin Cancer Res 2006;12:281-288.